Title

Parallel ICA of FDG-PET and PiB-PET in three conditions with underlying Alzheimer's pathology

Authors

Laforce, Robert

Tosun, Duygu

Ghosh, Pia

et al.

Publication Date

2014

DOI

10.1016/j.nicl.2014.03.005

Peer reviewed

NeuroImage: Clinical 4 (2014) 508–516

Contents lists available at ScienceDirect

NeuroImage: Clinical

journal homepage: www.elsevier.com/locate/ynicl

Parallel ICA of FDG-PET and PiB-PET in three conditions with underlying Alzheimer's pathology

Robert Laforce Jr[a,c,1,*], Duygu Tosun[b], Pia Ghosh[a,c], Manja Lehmann[a,c], Cindee M. Madison[a], Michael W. Weiner[b], Bruce L. Miller[c], William J. Jagust[a,d], Gil D. Rabinovici[a,c,d]

[a]Helen Wills Neuroscience Institute, University of California, Berkeley, CA, USA
[b]Center for Imaging of Neurodegenerative Diseases, Department of Radiology and Biomedical Imaging, University of California San Francisco, CA, USA
[c]Memory and Aging Center, Department of Neurology, University of California San Francisco, CA, USA
[d]Lawrence Berkeley National Laboratory, University of California, Berkeley, CA, USA

ARTICLE INFO

Article history:
Received 15 August 2013
Received in revised form 12 March 2014
Accepted 13 March 2014

Keywords:
Multivariate data analysis
Parallel ICA
Alzheimer's disease
Amyloid imaging
PiB-PET
FDG-PET
Functional connectivity
Networks

ABSTRACT

The relationships between clinical phenotype, β-amyloid (Aβ) deposition and neurodegeneration in Alzheimer's disease (AD) are incompletely understood yet have important ramifications for future therapy. The goal of this study was to utilize multimodality positron emission tomography (PET) data from a clinically heterogeneous population of patients with probable AD in order to: (1) identify spatial patterns of Aβ deposition measured by (^{11}C)-labeled Pittsburgh Compound B (PiB-PET) and glucose metabolism measured by FDG-PET that correlate with specific clinical presentation and (2) explore associations between spatial patterns of Aβ deposition and glucose metabolism across the AD population. We included all patients meeting the criteria for probable AD (NIA–AA) who had undergone MRI, PiB and FDG-PET at our center ($N = 46$, mean age 63.0 ± 7.7, Mini-Mental State Examination 22.0 ± 4.8). Patients were subclassified based on their cognitive profiles into an amnestic/dysexecutive group (AD-memory; $n = 27$), a language-predominant group (AD-language; $n = 10$) and a visuospatial-predominant group (AD-visuospatial; $n = 9$). All patients were required to have evidence of amyloid deposition on PiB-PET. To capture the spatial distribution of Aβ deposition and glucose metabolism, we employed parallel independent component analysis (pICA), a method that enables joint analyses of multimodal imaging data. The relationships between PET components and clinical group were examined using a Receiver Operator Characteristic approach, including age, gender, education and apolipoprotein E ϵ4 allele carrier status as covariates. Results of the first set of analyses independently examining the relationship between components from each modality and clinical group showed three significant components for FDG: a left inferior frontal and temporoparietal component associated with AD-language (area under the curve [AUC] 0.82, $p = 0.011$), and two components associated with AD-visuospatial (bilateral occipito-parieto-temporal [AUC 0.85, $p = 0.009$] and right posterior cingulate cortex [PCC]/precuneus and right lateral parietal [AUC 0.69, $p = 0.045$]). The AD-memory associated component included predominantly bilateral inferior frontal, cuneus and inferior temporal, and right inferior parietal hypometabolism but did not reach significance (AUC 0.65, $p = 0.062$). None of the PiB components correlated with clinical group. Joint analysis of PiB and FDG with pICA revealed a correlated component pair, in which increased frontal and decreased PCC/precuneus PiB correlated with decreased FDG in the frontal, occipital and temporal regions (partial $r = 0.75$, $p < 0.0001$). Using multivariate data analysis, this study reinforced the notion that clinical phenotype in AD is tightly linked to patterns of glucose hypometabolism but not amyloid deposition. These findings are strikingly similar to those of univariate paradigms and provide additional support in favor of specific involvement of the language network, higher-order visual network, and default mode network in clinical variants of AD. The inverse relationship between Aβ deposition and

Abbreviations: AD or AD-memory, Alzheimer's disease; AUC, area under the curve; AD-language or LPA, logopenic variant primary progressive aphasia; PCA or AD-visuospatial, posterior cortical atrophy; PCC, posterior cingulate cortex; PPC, posterior parietal cortex.

[1] Present address: Clinique Interdisciplinaire de Mémoire, Département des Sciences Neurologiques, CHU de Québec — Hôpital de l'Enfant-Jésus 1401, 18ième rue, Québec G1J 1Z4, Canada.

[*] Corresponding author:
E-mail address: robert.laforce@fmed.ulaval.ca (R. Laforce Jr).

http://dx.doi.org/10.1016/j.nicl.2014.03.005

glucose metabolism in partially overlapping brain regions suggests that Aβ may exert both local and remote effects on brain metabolism. Applying multivariate approaches such as pICA to multimodal imaging data is a promising approach for unraveling the complex relationships between different elements of AD pathophysiology.

1 Introduction

The relationships between amyloid, metabolism and clinical phenotype in Alzheimer's disease (AD) are incompletely understood. Previous studies have yielded mixed results within typical amnestic AD and across different AD phenotypes. For example, in three clinical variants of AD (AD-memory, AD-language, AD-visuospatial), clinical syndromes were strongly linked to patterns of glucose metabolism, whereas (^{11}C)-labeled Pittsburgh Compound B (PiB-PET) binding was similar across clinical phenotypes (Cohen et al., 2009; de Souza et al., 2011; Lehmann et al., 2013a; Leyton et al., 2011; Rabinovici et al., 2008; Rosenbloom et al., 2011). Correlations between increased β-amyloid and decreased metabolism have been found in some studies (Cohen et al., 2009; Edison et al., 2007; Engler et al., 2006) but not in others (Furst et al., 2012; Li et al., 2008). Some studies have suggested that the relationships between amyloid and glucose metabolism vary by brain region and disease state (Cohen et al., 2009; La Joie et al., 2012).

To date, most studies have investigated these relationships using univariate analyses, but this approach may fail to capture distributed variations across brain networks. A number of recent studies have demonstrated that multivariate statistical paradigms (e.g., principal component analysis or independent component analysis [ICA]), where distributed variations in multiple neuroimaging data and their inter-relationships are assessed together, provide a better framework for integrative analysis of imaging data. Multivariate techniques have been shown to be more sensitive for early diagnosis of AD and capture patterns of normal age-associated atrophy (Brickman et al., 2007). Parallel independent component analysis (pICA; Calhoun et al., 2006), a variation of ICA which allows estimation of independent components as well as multimodal patterns or mixed coefficients, has recently been used to study the mechanisms by which amyloid-β deposition leads to neurodegeneration and cognitive decline (Tosun et al., 2011). This is particularly relevant in light of possible distant (Bourgeat et al., 2010) rather than local (Cohen et al., 2009) effects of β-amyloid on glucose metabolism.

In this study we applied a multivariate approach to explore the relationships between metabolism and amyloid accumulation across AD phenotypes. To this end, we recruited patients with three phenotypes of AD cited in the new clinical diagnostic guidelines (McKhann et al., 2011): 1) a group of prototypical AD, or AD-memory, characterized by predominant episodic memory impairment and executive dysfunction (Dubois et al., 2007), 2) a group with language variant AD (AD-language, also called *logopenic variant primary progressive aphasia*) characterized by progressive word-finding difficulties and deficits in sentence repetition (Gorno-Tempini et al., 2004, 2011), and 3) a group with the visuospatial variant of AD (AD-visuospatial, also referred to as *posterior cortical atrophy*) marked by predominant visuospatial and visuoperceptual dysfunctions. We then applied pICA to 1) identify specific components from each modality that correlated with clinical presentation and 2) identify relationships between spatial patterns of PiB and FDG across AD patients. Based on previous results applying univariate statistics from our group and others, we hypothesized that FDG but not PiB would generate individual components that correlated with diagnosis. We further aimed to capture relationships between spatial patterns of glucose metabolism and amyloid deposition in this clinically and anatomically diverse cohort which may not be apparent using traditional univariate methods.

2. Subjects and methods

2.1. Subject selection and characteristics

We identified all patients seen at the University of California San Francisco (UCSF) Memory & Aging Center who met the criteria for probable AD according to the National Institute on Aging–Alzheimer's Association (NIA–AA) guidelines (McKhann et al., 2011), were PiB-positive and had available FDG and MRI scans. Patients were excluded if they had clinical or imaging evidence of previous stroke, or had a high burden of white matter hyperintensities (defined as Scheltens grade ≥ 4) (Scheltens et al., 1998). All patients were recruited between April 2005 and July 2011. Patients underwent a history and physical examination by a behavioral neurologist, a structured caregiver interview by a nurse, and a battery of neuropsychological tests (Kramer et al., 2003). All patients had mild-to-moderate dementia based on the Mini-Mental State Examination (MMSE; Folstein et al., 1975) and the Clinical Dementia Rating (CDR; Morris, 1993) scale. Diagnosis was made in a consensus clinical conference incorporating clinical and neuropsychological profiles but blinded to imaging data. Patients were subclassified as AD-memory, AD-language, and AD-visuospatial using published criteria (Gorno-Tempini et al., 2011; McKhann et al., 2011; Tang-Wai et al., 2004). The AD-memory group was composed of patients meeting the NIA–AA criteria for probable AD but not AD-language or AD-visuospatial criteria. The final cohort consisted of 27 patients with probable AD-memory, ten with AD-language and nine with AD-visuospatial (see Table 1).

2.2. Imaging

Acquisition parameters for all scanners have been described in previous publications (Mormino et al., 2012; Mueller et al., 2009; Rabinovici et al., 2007; Rosen et al., 2002; Zhou et al., 2012).

2.3. Structural imaging

T_1-weighted scans were collected at UCSF or Lawrence Berkeley National Laboratory (LBNL) on different MRI units, including two 1.5 T units (Magnetom Avanto System, Siemens Medical Systems, Erlangen, Germany; Magnetom VISION system, Siemens Inc., Iselin, NJ), a 3 T unit (Siemens Tim Trio scanner), and a 4 T unit (BrukerMedSpec). The proportions of subjects studied on each scanner were balanced across the three AD groups. In patients with multiple MRIs, the MRI closest to the date of the PET scan was used for data preprocessing.

Table 1
Patient characteristics.

Groups	AD-memory ($n = 27$)	AD-language ($n = 10$)	AD-visuospatial ($n = 9$)	p values
Age (mean, SD)	68.0 (10.7)	60.1 (5.7)	61.0 (6.7)	0.03*
M/F	16/11	5/5	6/3	0.84, ns
Education (mean, SD)	16.8 (2.5)	16.6 (3.4)	15.8 (3.5)	0.68, ns
ApoE ϵ4 status				0.07, ns
- Absent ϵ4	8	7	5	
- 1 ϵ4	14	3	2	
- 2 ϵ4	5	0	2	
MMSE /30	22.2 (5.0)	23.1 (3.7)	21.2 (5.8)	0.71, ns
CDR	0.96 (0.36)	0.55 (0.16)	0.67 (0.35)	0.002*
CDR-SB	6.2 (3.4)	3.0 (1.8)	4.6 (2.7)	0.02*

Abbreviations: Alzheimer's disease (AD); standard deviation (SD); apolipoprotein E ϵ4 allele (ApoE ϵ4); Mini-Mental State Examination (MMSE); Clinical Dementia Rating (CDR); Clinical Dementia Rating Sum of Boxes (CDR-SB).
*$p < 0.05$.

2.4. Positron emission tomography radiochemistry and acquisition

[^{11}C]PiB was synthesized at the LBNL Biomedical Isotope Facility using a previously published protocol. [^{18}F]FDG was purchased from a commercial vendor (IBA Molecular). PET scans were performed at LBNL using a Siemens ECAT EXACT HR PET scanner in 3-dimensional acquisition mode. 90 min of dynamic PiB data and 30 min of FDG data ($t = 30$–60 min post-injection, minimum of 2 h after PiB injection) were obtained. Ten-minute transmission scans for attenuation correction were obtained either immediately before or after each [^{11}C]PiB and [^{18}F]FDG scan. PET data were reconstructed using an ordered subset expectation–maximization algorithm with weighted attenuation. Images were smoothed with a 4 mm Gaussian kernel with scatter correction. All images were evaluated before analysis for patient motion and adequacy of statistical counts.

2.5. Image processing

All image pre-processing was performed in Statistical Parametric Mapping version 8 (SPM8; http://www.fil.ion.ucl.ac.uk/spm). Reference regions were defined in native MRI space for each subject using subcortical parcellations from FreeSurfer 4.5 (http://surfer.nmr.mgh.harvard.edu). FDG-PET frames were summed and standardized uptake value ratios (SUVR) were calculated by normalizing the summed FDG image to mean activity in the pons for each subject. For PiB, voxel-wise distribution volume ratios (DVRs) were calculated using Logan graphical analysis (Logan et al., 1996) with the gray matter cerebellum time–activity curve used as a reference tissue input function ($t = 35$–90 min) (Price et al., 2005).

2.6. Spatial normalization

PiB and FDG data were co-registered to the subject's skull stripped T_1-weighted MRI. To allow across-subject comparisons, each subject's T_1-weighted MRI was normalized to MNI (Montreal Neurological Institute) space using the skull stripped ch2 template, and the derived normalization parameters were applied to the subject's co-registered PiB and FDG volumes. All normalized images were smoothed with a 12-mm Gaussian kernel.

2.7. Visual inspection

Voxel-wise PiB DVR images from all subjects were qualitatively assessed by an experienced PET researcher (W.J.J.) blinded to clinical diagnosis. Scans were read visually as positive or negative for cortical PiB. A positive scan was defined as a DVR image in which uptake was substantially greater in the cortex than in the white matter. Visual inspection based on these criteria has been validated previously as a reproducible and reliable estimate of increased PiB uptake when compared with quantitative analysis (Mormino et al., 2012; Ng et al., 2007; Rabinovici et al., 2011).

2.8. Parallel ICA

We analyzed PiB and FDG data jointly and took all image voxels into account simultaneously using pICA (Fusion ICA Toolbox: Calhoun et al., 2006; Rachakonda et al., 2008). The mathematical foundations of pICA are described in detail in Liu et al. (2009). In this framework, pICA applied to multimodality imaging data aims to identify independent components in each image modality as well as the relationships of these independent components across image modalities. Briefly, ICA is run on each modality and a correlation measure is enforced between the mixing coefficients of modalities during the analysis. In the context of this study, pICA identified spatially independent components of PiB and FDG while simultaneously revealing the largest variations across patients that PiB and FDG had in common. The number of significant independent components in each modality was estimated using both the Akaike information criterion (AIC) and the minimum description length criterion. As a well-accepted order selection criterion, AIC maximizes the log-likelihood of the observed data based on the independent component set, with a penalty term that is directly proportional to the total number of independent components. The independent component set with the lowest AIC value is selected for a balance between the accuracy of fitting and the complexity of the independent component model. For each modality, the loading parameters expressing the contribution of each independent component to the variance across subjects were estimated. Each independent component for each modality was scaled to unit standard deviation, yielding z-score maps in the MNI template space. Because FDG-PET data is interpreted in terms of hypometabolism and PiB-PET data in terms of increased tracer retention, all FDG data were inverted (sign reversed). All component maps were thresholded at a z-score level of $|z| \geq 2.5$ (99.4% cumulative probability) for visualization purposes.

Based on these loading parameters, we computed Pearson's correlation coefficients for all pairs of PiB and FDG independent components while further accounting for variations in age, gender, education and apolipoprotein E ϵ4 allele (ApoE ϵ4) carrier status. The Pearson's correlation coefficients were then used to identify significant relationships between brain amyloid-β accumulation and hypometabolism after correction for multiple comparisons using a false discovery rate (FDR) at a significance level of $p < 0.05$. Relationship to clinical group was examined using a Receiver Operator Characteristic approach, including age, gender, education, and ApoE ϵ4 (present/absent) as covariates. The ROC analyses assessed the contribution of each component separately to the classification of one clinical group from the other two (e.g., AD-memory versus AD-language and AD-visuospatial) within the general linear model framework, using the

logit function as link between the linear predictor variable (i.e., loading parameters of a component) and group as binomial outcome variable (clinical group of interest = 1 versus rest = 0).

2.9. Statistical analysis

Group differences in demographic variables were examined using one-way analysis of variance or the Mann–Whitney *U* test. As appropriate statistical analyses were implemented in R Software (http://www.r-project.org/). This study was approved by the University of California, Berkeley, University of California, San Francisco, and Lawrence Berkeley National Laboratory institutional review boards for human research.

3. Results

3.1. Patient characteristics

Patient characteristics are shown in Table 1. Patients with AD-memory were significantly older at PET and were more impaired on CDR and CDR Sum-of-Boxes (CDR-SB) ($p = 0.03$). No significant differences were found in gender, education, ApoE ϵ4 status or MMSE.

3.2. Neuropsychological evaluations

Neuropsychological test batteries were available for most patients (see Table 2). The mean interval between cognitive testing and PET was 131 days (SD 207.6 days). As expected, AD-memory patients performed poorly on verbal and visual memory tasks ($p = 0.03$ on the California Verbal Learning Test 10-minute delayed recall, and $p = 0.01$ on the modified Rey 10-minute delayed recall), whereas AD-visuospatial patients showed lower performance on visuospatial tasks ($p = 0.02$ for modified Rey copy). The AD-language group performed significantly worse on sentence repetition ($p = 0.003$), consistent with the deficits in auditory working memory previously reported in this group.

3.3. Individual FDG and PiB components

The number of estimated components using the AIC in our observed data from 46 subjects was eight for the FDG-PET feature and seven for the PiB-PET feature. Three of the eight FDG components were associated with a particular clinical group with significant predictor accuracy. A left inferior frontal and left temporoparietal hypometabolism component was associated with AD-language with an area under the curve (AUC) of 0.82 ($p = 0.011$) (Fig. 1A). Two components correlated with AD-visuospatial, one involving bilateral occipito-parieto-temporal hypometabolism (Fig. 1B) and another involving right posterior cingulate cortex (PCC)/precuneus and right lateral parietal hypometabolism (Fig. 1C) with AUC measures of 0.85 ($p = 0.009$) and 0.69 ($p = 0.045$), respectively. A fourth component correlated at a trend level with AD-memory (Fig. 1D). This component included predominantly bilateral inferior frontal, cuneus and inferior temporal, and right inferior parietal hypometabolism (AUC of 0.65, $p = 0.062$). The remaining FDG components showed no association with clinical presentation (data not shown). These included two components showing bilateral cerebellar hypometabolism, one with bilateral medial orbito-frontal, inferior frontal, and right superior frontal hypometabolism, and one with cerebellar and superior frontal hypometabolism. Supplementary Figs. S1–S4 illustrate the associations with clinical groups.

None of the seven estimated PiB components (left PCC and lateral parietal; right parieto-temporal; bilateral cerebellar; bilateral inferior frontal; bilateral temporal, frontal, parietal, PCC/precuneus, and cerebellar; bilateral fronto-orbital and PCC/precuneus; bilateral fronto-orbital and middle frontal) were significant predictors in classifying clinical groups after adjusting for age, sex, education, and ApoE ϵ4.

Mean FDG and PiB images of each of the three groups are provided as Supplementary Figs. S5–S10 to allow for qualitative comparison of PET patterns across groups.

3.4. Joint FDG and PiB components

We also explored the joint predictive value of FDG and PiB independent components in correctly classifying a given diagnostic group from the rest and among all possible pair combinations identified, with paired glucose metabolism and amyloid deposition components providing significant improvement in classification accuracy relative to the ones based on unimodal components. The AD-memory related hypometabolism component (shown in Fig. 1D) jointly with a PiB component with amyloid deposition in the left posterior parietal cortex and lateral parietal regions provided an AUC measure of 0.76 (Supplementary Fig. S11), significantly larger than single modality (AUC of 0.65, $p < 0.01$). The same PiB component when considered jointly with the AD-language related hypometabolism component (Fig. 1A) significantly ($p < 0.01$) improved the classification accuracy from AUC = 0.82 to AUC = 0.87 (Supplementary Fig. S12). A more diffuse PiB component including temporal, parietal, PCC/precuneus, and lateral and medial frontal amyloid deposition when considered jointly with the first AD-visuospatial related hypometabolism component shown in Fig. 1B in a multimodal principal component analysis diagnosis prediction model increased the unimodal hypometabolism AUC measure of 0.85–0.88 ($p < 0.01$) (Supplementary Fig. S13).

3.5. Correlated FDG and PiB components

We found a significant and spatially distributed component pair across all subjects, depicting an association between FDG and PiB. In this component pair, increased frontal and decreased PCC/precuneus PiB binding was correlated with decreased FDG uptake in the frontal, occipital and temporal regions (Fig. 2). This component pair showed a partial correlation of 0.75, with an FDR-corrected significance level of $p < 10^{-6}$. The adjusted R^2 value of the fitted model for this component pair was 0.56 with $p < 10^{-8}$. The FDG component in this pair was the same component that showed, on its own, a trend correlation with the AD-memory phenotype ($p = 0.062$, Fig. 1D). The PiB component was not correlated with a specific phenotype (as was true for all PiB components). This combined PiB-FDG component did not correlate with a specific group.

4. Discussion

In this study we applied pICA to FDG-PET and PiB-PET data in an attempt to better understand the relationships between glucose metabolism, amyloid aggregation and clinical phenotype in AD. We found that memory, language, and visuospatial-predominant clinical variants of AD were associated with independent components of glucose metabolism but not with specific patterns of β-amyloid deposition. FDG and PiB jointly improved the classification of one variant from others, though the added effect of joint FDG-PiB versus FDG alone was relatively small. Multivariate analyses further revealed an inverse relationship between Aβ deposition and glucose metabolism in the frontal cortex and PCC/precuneus, providing insight into the biological interplay between these two biomarkers in key regions of AD-related degeneration.

4.1. Replicating previous univariate efforts using a multivariate approach

Using pICA we replicated previous findings from univariate analyses demonstrating that the clinical phenotype in AD is strongly linked to anatomic patterns of glucose hypometabolism but not to the spatial distribution of amyloid deposition (Lehmann et al.,

Table 2
Neuropsychological profiles.

Neuropsychological tests	AD-memory ($n = 27$)	AD-language ($n = 10$)	AD-visuospatial ($n = 9$)	p values
Memory				
CVLT-SF total learning (/36)	15.4 (6.9)	17.3 (6.8)	15.3 (3.8)	0.70
CVLT-SF 10-min recall (/9)	1.1 (2.2)	3.5 (2.6)	2.1 (2.3)	0.03*
Modified Rey 10-min recall (/17)	2.2 (3.3)	6.0 (3.4)	2.9 (3.6)	0.01*
Language				
Boston naming test (/15)	10.4 (3.9)	9.8 (4.1)	10.6 (4.8)	0.91
Syntax comprehension (/5)	3.3 (1.1)	3.0 (1.3)	2.1 (1.9)	0.10
Letter fluency (D words)	9.5 (5.0)	5.9 (3.3)	8.9 (4.0)	0.12
Category fluency (animals)	8.9 (4.4)	8.6 (4.1)	9.3 (4.6)	0.93
Sentence repetition (/5)	3.3 (1.6)	1.5 (0.7)	3.2 (1.0)	0.003*
Repetition and working memory				
Digit span forward (/9)	5.1 (1.2)	4.2 (0.8)	5.3 (1.0)	0.18
Digit span backward (/8)	3.7 (1.7)	3.0 (0.7)	2.4 (0.5)	0.05
Executive functions				
Modified trails B correct lines/min	10.2 (11.1)	9.1 (7.2)	5.7 (5.3)	0.56
Stroop interference no. correct	17.3 (14.5)	16.9 (10.5)	14.6 (12.0)	0.90
Visuospatial				
Modified Rey copy (/17)	11.8 (4.7)	14.0 (3.8)	7.6 (4.9)	0.02*
VOSP number location (/10)	6.9 (3.2)	8.0 (2.9)	4.2 (2.3)	0.06
CATS				
Affect naming (/16)	11.7 (2.1)	12.3 (2.6)	12.0 (1.0)	0.82
Face matching (/12)	10.7 (0.5)	11.7 (0.5)	9.7 (2.0)	0.13
Calculation				
Arithmetics, written (/5)	3.3 (1.5)	3.0 (0.7)	2.8 (1.2)	0.51

Abbreviations: California Verbal Learning Test (CVLT); Comprehensive Affect Testing System (CATS); Visual Object and Space Perception (VOSP). Missing data: modified Rey copy: 1 AD-visuospatial; Boston naming: 2 AD-memory; syntax comprehension: 2 AD-memory, 1 AD-visuospatial; letter fluency: 1 AD-memory; digit span forward: 20 AD-memory, 4 AD-language, 5 AD-visuospatial; digit span backward: 1 AD-memory; modified trails: 7 AD-memory, 1 AD-language, 2 AD-visuospatial; Stroop: 6 AD-memory, 2 AD-language, 2 AD-visuospatial; VOSP number location: 3 AD-memory, 1 AD-language, 3 AD-visuospatial; arithmetic: 1 AD-visuospatial; face matching: 10 AD-memory, 3 AD-language, 3 AD-visuospatial; affect naming: 10 AD-memory, 3 AD-language, 4 AD-visuospatial.
*$p < 0.05$.

2013a). Specifically, three independent glucose metabolism components were associated with specific clinical variants with high predictor accuracy. First, a left inferior frontal and temporoparietal hypometabolism component was associated with AD-language. This is congruent with previous studies demonstrating asymmetric left temporoparietal atrophy and hypometabolism in AD-language (Gorno-Tempini et al., 2004; Rabinovici et al., 2008). Two AD-visuospatial related components were found, one involving bilateral occipito-parieto-temporal hypometabolism and right PCC/lateral parietal hypometabolism. Again, this is in agreement with previous literature showing focal patterns of neurodegeneration with bilateral occipito-parieto-temporal atrophy and hypometabolism in AD-visuospatial (Lehmann et al., 2011; Migliaccio et al., 2009; Rosenbloom et al., 2011; Whitwell et al., 2007). The AD-memory variant was not significantly associated with a specific FDG component. This may be due to inclusion of relatively young AD patients in this group — patients with early age-of-onset AD show relatively diffuse cognitive deficits, including involvement of language and visuospatial domains that overlaps with the more focal AD-language and AD-visuospatial groups (Lehmann et al., 2012; Migliaccio et al., 2009). However, at a trend level we found an association with a primarily frontal component, consistent with previous studies demonstrating that frontal involvement may distinguish this variant of AD from others (Lehmann et al., 2013a and b; Migliaccio, 2009).

In contrast with the syndrome-specific FDG components, PiB binding was similar across clinical syndromes. The fact that none of the seven estimated amyloid deposition components were significant predictors of clinical conditions is congruent with most studies, which have reported overlapping patterns of amyloid accumulation in distinct variants of AD (Lehmann et al., 2013a). Although single case reports and small series initially reported atypical binding patterns in AD-language and AD-visuospatial (Ng et al., 2007), larger series have found a diffuse pattern indistinguishable from typical AD and dissociated from their focal structural and metabolic signatures (de Souza et al., 2011; Lehmann et al., 2013a; Leyton et al., 2011; Rabinovici et al., 2008; Rosenbloom et al., 2011). Other studies comparing PiB binding in early and late age-of-onset AD found that differences in cognitive profiles could not be explained by the distribution or burden of PiB, which was identical in the groups (Rabinovici et al., 2010). Altogether, our multivariate pICA strategy replicated previous findings using mass-univariate voxel-wise group comparisons.

4.2. Linking metabolic patterns to specific networks of degeneration in the brain

There is accumulating evidence that neurodegeneration occurs in specific networks in the brain (Seeley et al., 2009; Zhou et al., 2012). A recent PET study (Lehmann et al., 2013a) showed that patterns of glucose hypometabolism in early-onset AD (EOAD), AD-language, and AD-visuospatial matched the network templates of executive-control, language, and visual networks, respectively. Notably, the FDG component linked by pICA in our study to AD-language bears a striking resemblance to the language network as identified by task-based or task-free fMRI (Fig. 1A; Shirer et al., 2012; Smith et al., 2009). The FDG components linked with AD-visuospatial closely resemble a high-order visual network (Fig. 1B) and a right hemisphere posterior default mode network (DMN; Fig. 1C). These findings support a recently proposed model postulating that the emergence of heterogeneous AD phenotypes is related to the involvement of specific functional networks that converge in the DMN (Lehmann et al., 2013b). This model integrates the hypothesis that aggregation of amyloid-beta may be driven by total flow of neuronal activity (yielding diffuse and symmetric patterns of PiB binding throughout 'cortical hubs'), whereas

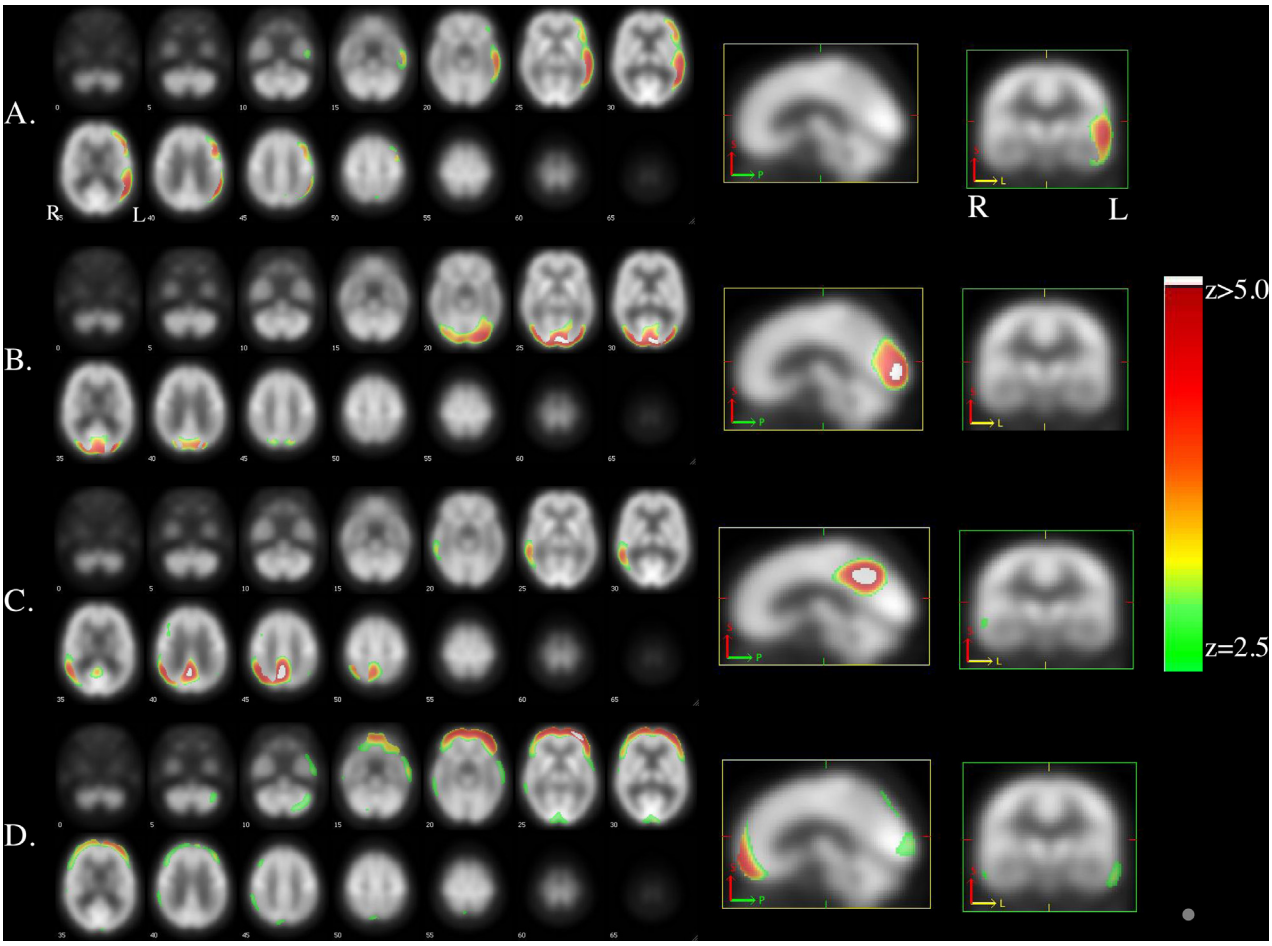

Fig. 1. A) AD-language associated component included left inferior frontal and temporoparietal hypometabolism, B) AD-visuospatial related component 1 involved bilateral occipito-parieto-temporal hypometabolism, C) AD-visuospatial related component 2 involved right PCC/precuneus and right lateral parietal hypometabolism, and D) AD-memory associated component included predominantly bilateral inferior frontal, but also cuneus and inferior temporal, and right inferior parietal hypometabolism. Images are presented on a study-specific template in radiological convention. Supplementary Figures S1–S4 illustrate the associations with clinical groups.

the aggregation of tau may be driven by transneuronal spread, generating patterns of neurodegeneration that coincide with specific functional networks and ultimately lead to specific clinical phenotypes (de Calignon et al., 2012; Seeley et al., 2009; Zhou et al., 2012).

4.3. *Spatially distributed relationship between amyloid deposition and metabolism*

An additional goal of this study was to explore spatially disparate relationships between patterns of Aβ deposition and glucose metabolism across a heterogenous AD population. We found a significant pICA component pair, in which increased frontal and decreased PCC/precuneus β-amyloid deposition was correlated with decreased glucose metabolism in frontal, occipital and lateral temporal regions. The patterns of PiB and FDG showed partial overlap in medial prefrontal cortex, but were otherwise spatially disparate. In the context of current models of the AD pathophysiologic cascade (Jack et al., 2013), these findings suggest that Aβ may exert both local and remote effects on brain metabolism, the latter potentially due to deafferentation of remote areas (Bourgeat et al., 2010). Traditional univariate approaches have similarly demonstrated both local and remote correlations between PiB and FDG (Cohen et al., 2009; Edison et al., 2007; Engler et al., 2006). Our results are further congruent with a recent report in mild cognitive impairment, which showed via pICA that increased amyloid-β burden in the left precuneus/cuneus and medial-temporal regions was associated with increased brain atrophy rates in the left medial-temporal and parietal regions, while increased amyloid- β burden in bilateral precuneus/cuneus and parietal regions was associated with increased brain atrophy rates in the right medial temporal regions (Tosun et al., 2011).

Intriguingly, the PiB component in this pair consisted of *increased* medial frontal and *decreased* PCC/precuneus binding. It is important not to misinterpret this finding as evidence of low amyloid in PCC/precuneus — rather it must be interpreted as a dynamic relationship between regional levels of amyloid accumulation (high in the medial frontal cortex, low in the PCC/precuneus) and brain metabolism. This raises the possibility that variations in amyloid aggregation within key regions of the DMN may modulate the pattern of neurodegeneration in AD. Notably, hypometabolism in the prefrontal and occipital cortex typically occurs in advanced clinical stages of AD (Kim et al., 2005), whereas medial prefrontal amyloid aggregation may be an early event in the AD cascade (Sepulcre et al., 2013), further underscoring the relative resilience of the prefrontal cortex to AD pathology (Furst et al., 2012). While the reliability and significance of this observation will require further (and ideally longitudinal) study, our observation underscores the complexity of the relationship between amyloid and metabolism, which appears to vary by brain region and disease state (Cohen et al., 2009; La Joie et al., 2012). Future studies with larger sample sizes should also attempt to explore whether joint spatial relationships between PiB and FDG correlate with specific clinical features or neuropsychological profiles.

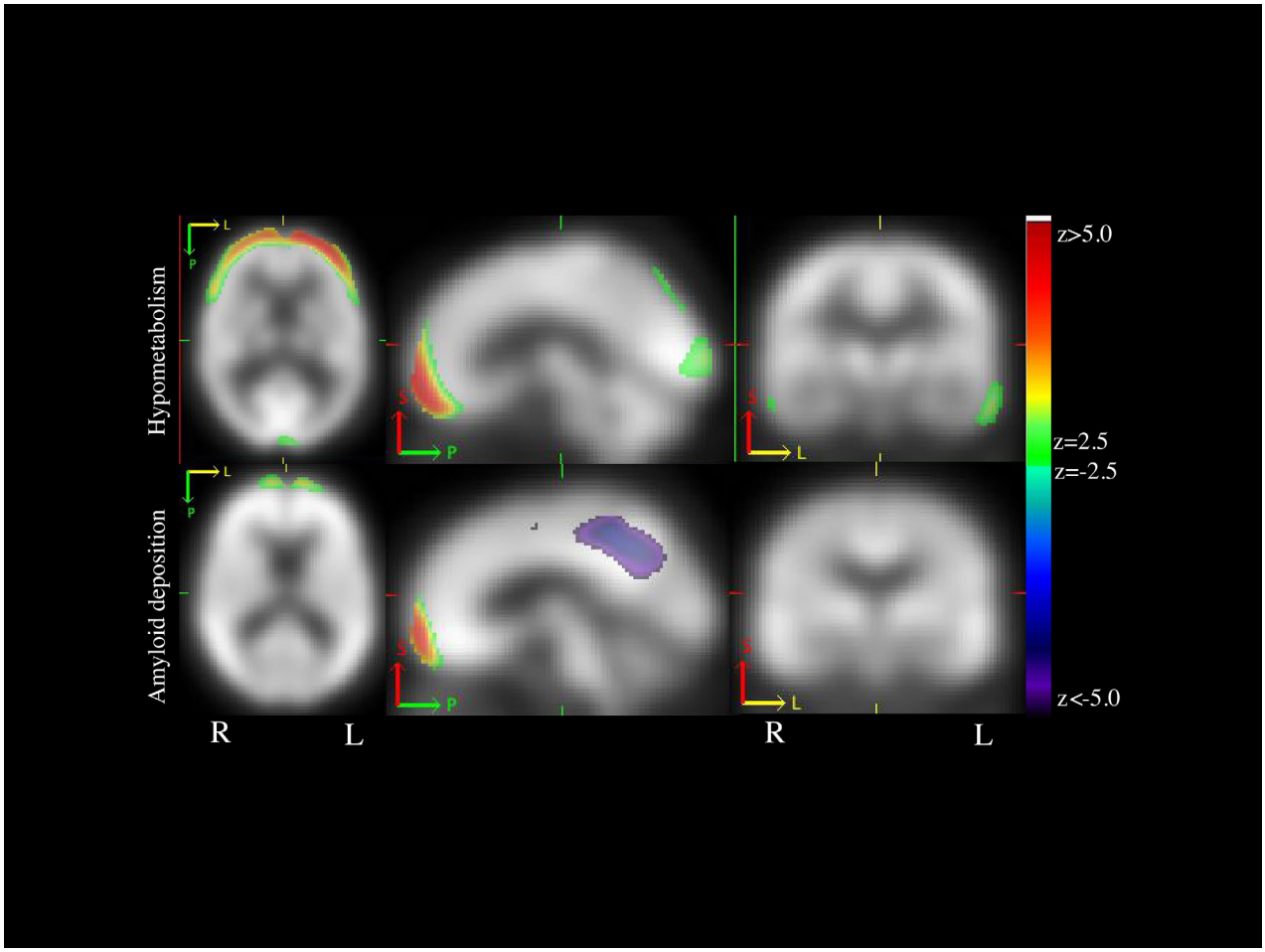

Fig. 2. Component pair depicting an association between hypometabolism and amyloid deposition. The spatial extent of this component pair showed that increased frontal and decreased PCC/precuneus β-amyloid deposition correlated with decreased glucose metabolism in the frontal, occipital and temporal regions. Images are presented on a study-specific template in radiological convention. Abbreviations. Amyloid beta (Aβ); Alzheimer's disease (AD); default mode network (DMN); posterior cingulate cortex (PCC).

4.4. Role of multivariate analyses

Use of multivariate techniques in the analysis of imaging data is gaining traction on the field. Multivariate approaches evaluate correlation/covariance of data across brain regions rather than proceeding on a voxel-by-voxel basis. They may be particularly helpful when integrating multiple imaging modalities that capture different elements of disease pathophysiology (Tosun et al., 2011). Unlike univariate approaches, which treat each voxel or region as a spatially independent unit, multivariate analyses can explicitly examine the inter-relationship among these units and allow for better inference of the biological interconnectivity among brain regions (Devanand et al., 2006; Eidelberg et al., 1991; Moeller and Eidelberg, 1997; see O'Toole et al., 2007 for a review). Thus, results can be more easily interpreted as a signature of neural networks, which may be a key element to understanding the heterogeneity and pathophysiology of neurodegenerative disease (Lehmann et al., 2013a and b; Seeley et al., 2009; Sepulcre et al., 2013; Zhang et al., 2012). Such approaches also provide greater statistical power when compared with univariate techniques, which are forced to employ very stringent, and often overly conservative, corrections for voxel-wise multiple comparisons. These strengths can be leveraged to improve diagnostic classification, as seen in our joint classification analysis, where the combination of PiB and FDG improved the discrimination of clinical variants compared to FDG alone (Habeck et al., 2008).

4.5. Limitations

This study has several limitations. While our patients met the NIA–AA criteria for high-likelihood AD, pathological confirmation of the diagnosis was not available. Our sample size was too small to explore relationships between individual components and specific cognitive tests. We could not include a structural imaging component because MRIs were performed on four different scanners with three different magnetic field strengths. We did not correct PET data for partial volume loss, because (1) we were interested in FDG as a marker of neurodegeneration (rather than glucose metabolism per se), especially in lieu of MRI data, such that it was advantageous to include the effects of atrophy and (2) atrophy correction of PiB data can introduce significant bias, and the utility and optimal methods are controversial (Thomas et al., 2011). In the past we have found identical results with and without atrophy correction examining similar relationships with univariate methods (Lehmann et al., 2013a; Rabinovici et al., 2010; Rosenbloom et al., 2011). pICA assumes that measurements in each image voxel are independent and that the overall noise is identically distributed assumptions which may not be fully met by PET data. PiB is a relatively novel tracer and may have ceiling effects or undescribed binding interactions that may limit data interpretation. Furthermore, PiB binds to fibrillar forms of Aβ but not to the more toxic soluble Aβ aggregates. Finally, as discussed above, our cross-sectional design limits inferences about cause/effect and temporal relationships between amyloid aggregation and brain metabolism —

further, longitudinal studies will be needed to further clarify these issues.

5. Conclusions

Multivariate analysis of PET data from a clinically heterogeneous population of patients with probable AD showed that clinical phenotype correlated with independent components of glucose metabolism but not with patterns of β-amyloid deposition. These findings are strikingly similar to those derived from univariate paradigms and provide additional support for involvement of specific functional networks in clinical variants of AD via Aβ-independent mechanisms. pICA revealed that β-amyloid deposition and glucose metabolism show both local and spatially disparate relationships across the brain, highlighting the complexity of the relationship between molecular pathology and neurodegeneration in AD. Further clarifying the relations between these processes is of utmost importance given the effort to develop treatments targeting specific events in the AD pathophysiological cascade.

Conflicts of interest

RL has nothing to disclose. GDR received consulting fees from Eli Lilly and GE Healthcare and receives grant support from Avid Radiopharmaceuticals, a wholly-owned subsidiary of Eli Lilly and Company that is developing amyloid PET tracers for commercial purposes. WJJ has consulted for Synarc and for Hoffman LaRoche.

Acknowledgments

We would like to thank all patients and their families who participated in this study. We are also grateful to Dr Hwamee Oh for her advice on multivariate statistical issues. This work was supported by a Fellowship grant from Fonds de Recherche en Santé du Québec (to RL), National Institute on Aging grants K23-AG031861 (to GDR), P01-AG1972403 and P50-AG023501 (to BLM), R01-AG027859 (to WJJ); Alzheimer's Association grant NIRG-07-59422 (to GDR); Alzheimer's Research UK grant ART-TRFUS2011-2 (to ML); John Douglas French Alzheimer's Foundation grant (to GDR); State of California Department of Health Services Alzheimer's Disease Research Center of California grant 04-33516 (to BLM); and Hellman Family Foundation grant (to GDR).

Supplementary material

Supplementary material associated with this article can be found, in the online version, at doi:10.1016/j.nicl.2014.03.005.

References

Bourgeat, P., Chételat, G., Villemagne, V.L., Fripp, J., Raniga, P., Pike, K., et al. 2010. Beta-amyloid burden in the temporal neocortex is related to hippocampal atrophy in elderly subjects without dementia. Neurology 74 (2), 121–7. http://dx.doi.org/10.1212/WNL.0b013e3181c918b5, 20065247.

Brickman, A.M., Habeck, C., Zarahn, E., Flynn, J., Stern, Y., 2007. Structural MRI covariance patterns associated with normal aging and neuropsychological functioning. Neurobiology of Aging 28 (2), 284–95. http://dx.doi.org/10.1016/j.neurobiolaging.2005.12.016, 16469419.

Calhoun, V.D., Adali, T., Kiehl, K.A., Astur, R., Pekar, J.J., Pearlson, G.D., 2006. A method for multitask fMRI data fusion applied to schizophrenia. Human Brain Mapping 27 (7), 598–610. http://dx.doi.org/10.1002/hbm.20204, 16342150.

Cohen, A.D., Price, J.C., Weissfeld, L.A., James, J., Rosario, B.L., Bi, W., et al. 2009. Basal cerebral metabolism may modulate the cognitive effects of Abeta in mild cognitive impairment: an example of brain reserve. Journal of Neuroscience: the Official Journal of the Society for Neuroscience 29 (47), 14770–8. http://dx.doi.org/10.1523/JNEUROSCI.3669-09.2009, 19940172.

de Calignon, A., Polydoro, M., Suárez-Calvet, M., William, C., Adamowicz, D.H., Kopeikina, K.J., et al. 2012. Propagation of tau pathology in a model of early Alzheimer's disease. Neuron 73 (4), 685–97. http://dx.doi.org/10.1016/j.neuron.2011.11.033, 22365544.

de Souza, L.C., Corlier, F., Habert, M.O., Uspenskaya, O., Maroy, R., Lamari, F., et al. 2011. Similar amyloid-beta burden in posterior cortical atrophy and Alzheimer's disease. Brain: a Journal of Neurology 134 (7), 2036–43. http://dx.doi.org/10.1093/brain/awr130, 21705422.

Devanand, D.P., Habeck, C.G., Tabert, M.H., Scarmeas, N., Pelton, G.H., Moeller, J.R., et al. 2006. PET network abnormalities and cognitive decline in patients with mild cognitive impairment. Neuropsychopharmacology: Official Publication of the American College of Neuropsychopharmacology 31 (6), 1327–34, 16292330.

Dubois, B., Feldman, H.H., Jacova, C., Dekosky, S.T., Barberger-Gateau, P., Cummings, J., et al. 2007. Research criteria for the diagnosis of Alzheimer's disease: revising the NINCDS–ADRDA criteria. Lancet Neurology 6 (8), 734–46. http://dx.doi.org/10.1016/S1474-4422(07)70178-3, 17616482.

Edison, P., Archer, H.A., Hinz, R., Hammers, A., Pavese, N., Tai, Y.F., et al. 2007. Amyloid, hypometabolism, and cognition in Alzheimer disease: an [^{11}C]PIB and [^{18}F]FDG PET study. Neurology 68 (7), 501–8. http://dx.doi.org/10.1212/01.wnl.0000244749.20056.d4, 17065593.

Eidelberg, D., Dhawan, V., Moeller, J.R., Sidtis, J.J., Ginos, J.Z., Strother, S.C., et al. 1991. The metabolic landscape of corticobasal ganglionic degeneration: regional asymmetries studied with positron emission tomography. Journal of Neurology, Neurosurgery, and Psychiatry 54 (10), 856–62. http://dx.doi.org/10.1136/jnnp.54.10.856, 1744638.

Engler, H., Forsberg, A., Almkvist, O., Blomquist, G., Larsson, E., Savitcheva, I., et al. 2006. Two-year follow-up of amyloid deposition in patients with Alzheimer's disease. Brain: a Journal of Neurology 129 (11), 2856–66. http://dx.doi.org/10.1093/brain/awl178, 16854944.

Folstein, M.F., Folstein, S.E., McHugh, P.R., 1975. "Mini-Mental State". A practical method for grading the cognitive state of patients for the clinician. Journal of Psychiatric Research 12 (3), 189–98. http://dx.doi.org/10.1016/0022-3956(75)90026-6, 1202204.

Furst, A.J., Rabinovici, G.D., Rostomian, A.H., Steed, T., Alkalay, A., Racine, C., et al. 2012. Cognition, glucose metabolism and amyloid burden in Alzheimer's disease. Neurobiology of Aging 33 (2), 215–25. http://dx.doi.org/10.1016/j.neurobiolaging.2010.03.011, 20417582.

Gorno-Tempini, M.L., Dronkers, N.F., Rankin, K.P., Ogar, J.M., Phengrasamy, L., Rosen, H.J., et al. 2004. Cognition and anatomy in three variants of primary progressive aphasia. Annals of Neurology 55 (3), 335–46. http://dx.doi.org/10.1002/ana.10825, 14991811.

Gorno-Tempini, M.L., Hillis, A.E., Weintraub, S., Kertesz, A., Mendez, M., Cappa, S.F., et al. 2011. Classification of primary progressive aphasia and its variants. Neurology 76 (11), 1006–14. http://dx.doi.org/10.1212/WNL.0b013e31821103e6, 21325651.

Habeck, C., Foster, N.L., Perneczky, R., Kurz, A., Alexopoulos, P., Koeppe, R.A., et al. 2008. Multivariate and univariate neuroimaging biomarkers of Alzheimer's disease. NeuroImage 40 (4), 1503–15. http://dx.doi.org/10.1016/j.neuroimage.2008.01.056, 18343688.

Jack, C.R. Jr., Knopman, D.S., Jagust, W.J., Petersen, R.C., Weiner, M.W., Aisen, P.S., et al. 2013. Tracking pathophysiological processes in Alzheimer's disease: an updated hypothetical model of dynamic biomarkers. Lancet Neurology 12 (2), 207–16. http://dx.doi.org/10.1016/S1474-4422(12)70291-0, 23332364.

Kim, E.J., Cho, S.S., Jeong, Y., Park, K.C., Kang, S.J., Kang, E., et al. 2005. Glucose metabolism in early onset versus late onset Alzheimer's disease: an SPM analysis of 120 patients. Brain: a Journal of Neurology 128 (8), 1790–801. http://dx.doi.org/10.1093/brain/awh539, 15888536.

Kramer, J.H., Jurik, J., Sha, S.J., Rankin, K.P., Rosen, H.J., Johnson, J.K., et al. 2003. Distinctive neuropsychological patterns in frontotemporal dementia, semantic dementia, and Alzheimer disease. Cognitive and Behavioral Neurology: Official Journal of the Society for Behavioral and Cognitive Neurology 16 (4), 211–18. http://dx.doi.org/10.1097/00146965-200312000-00002, 14665820.

La, Joie R., Perrotin, A., Barré, L., Hommet, C., Mézenge, F., Ibazizene, M., et al. 2012. Region-specific hierarchy between atrophy, hypometabolism, and β-amyloid (Aβ) load in Alzheimer's disease dementia. Journal of Neuroscience: the Official Journal of the Society for Neuroscience 32 (46), 16265–73. http://dx.doi.org/10.1523/JNEUROSCI.2170-12.2012, 23152610.

Lehmann, M., Crutch, S.J., Ridgway, G.R., Ridha, B.H., Barnes, J., Warrington, E.K., et al. 2011. Cortical thickness and voxel-based morphometry in posterior cortical atrophy and typical. Alzheimer'S Disease. Neurobiology of Aging 32 (8), 1466–76. http://dx.doi.org/10.1016/j.neurobiolaging.2009.08.017.

Lehmann, M., Barnes, J., Ridgway, G.R., Ryan, N.S., Warrington, E.K., Crutch, S.J., et al. 2012. Global gray matter changes in posterior cortical atrophy: a serial imaging study. Alzheimer's & Dementia: the Journal of the Alzheimer's Association 8, 502–12. http://dx.doi.org/10.1016/j.jalz.2011.09.22510.1016/j.jalz.2012.05, 22365384.

Lehmann, M., Ghosh, P.M., Madison, C., Laforce, R. Jr., Corbetta-Rastelli, C., Weiner, M.W., et al. 2013. Diverging patterns of amyloid deposition and hypometabolism in clinical variants of probable Alzheimer's disease. Brain: a Journal of Neurology 136 (3), 844–58. http://dx.doi.org/10.1093/brain/aws327, 23358601.

Lehmann, M., Madison, C.M., Ghosh, P.M., Seeley, W.W., Mormino, E., Greicius, M.D., et al. 2013. Intrinsic connectivity networks in healthy subjects explain clinical variability in Alzheimer's disease. Proceedings of the National Academy of Sciences of the United States of America 110 (28), 11606–11. http://dx.doi.org/10.1073/pnas.1221536110, 23798398.

Leyton, C.E., Villemagne, V.L., Savage, S., Pike, K.E., Ballard, K.J., Piguet, O., et al. 2011. Subtypes of progressive aphasia: application of the international consensus criteria and validation using beta-amyloid imaging. Brain: a Journal of Neurology 134 (10), 3030–43. http://dx.doi.org/10.1093/brain/awr216, 21908392.

Li, Y., Rinne, J.O., Mosconi, L., Pirraglia, E., Rusinek, H., DeSanti, S., et al. 2008. Regional analysis of FDG and PIB-PET images in normal aging, mild cognitive impairment, and Alzheimer's disease. European Journal of Nuclear Medicine and Molecular imaging 35 (12), 2169–81. http://dx.doi.org/10.1007/s00259-008-0833-y, 18566819.

Liu, J., Pearlson, G., Windemuth, A., Ruano, G., Perrone-Bizzozero, N.I., Calhoun, V., 2009. Combining fMRI and SNP data to investigate connections between brain function and genetics using parallel ICA. Human Brain Mapping 30 (1), 241–55. http://dx.doi.org/10.1002/hbm.20508, 18072279.

Logan, J., Fowler, J.S., Volkow, N.D., Wang, G.J., Ding, Y.S., Alexoff, D.L., 1996. Distribution volume ratios without blood sampling from graphical analysis of PET data. Journal of Cerebral Blood Flow and Metabolism: Official Journal of the International Society of Cerebral Blood Flow and Metabolism 16 (5), 834–40, 8784228.

McKhann, G.M., Knopman, D.S., Chertkow, H., Hyman, B.T., Jack, C.R. Jr., Kawas, C.H., et al. 2011. The diagnosis of dementia due to Alzheimer's disease: recommendations from the National Institute on Aging-Alzheimer's Association workgroups on diagnostic guidelines for Alzheimer's disease. Alzheimer's & Dementia: the Journal of the Alzheimer's Association 7 (3), 263–9. http://dx.doi.org/10.1016/j.jalz.2011.03.005, 21514250.

Migliaccio, R., Agosta, F., Rascovsky, K., Karydas, A., Bonasera, S., Rabinovici, G.D., et al. 2009. Clinical syndromes associated with posterior atrophy: early age at onset AD spectrum. Neurology 73 (19), 1571–8. http://dx.doi.org/10.1212/WNL.0b013e3181c0d427, 19901249.

Moeller, J.R., Eidelberg, D., 1997. Divergent expression of regional metabolic topographies in Parkinson's disease and normal ageing. Brain: a Journal of Neurology 120 (12), 2197–206. http://dx.doi.org/10.1093/brain/120.12.2197, 9448575.

Mormino, E.C., Brandel, M.G., Madison, C.M., Rabinovici, G.D., Marks, S., Baker, S.L., et al. 2012. Not quite PIB-positive, not quite PIB-negative: slight PIB elevations in elderly normal control subjects are biologically relevant. Neuroimage 59 (2), 1152–60. http://dx.doi.org/10.1016/j.neuroimage.2011.07.098, 21884802.

Morris, J.C., 1993. The Clinical Dementia Rating (CDR): Current version and scoring rules. Neurology 43 (11), 2412–14. http://dx.doi.org/10.1212/WNL.43.11.2412-a10.1212/WNL.43.11.2412, 8232972.

Mueller, S.G., Laxer, K.D., Barakos, J., Cheong, I., Garcia, P., Weiner, M.W., 2009. Widespread neocortical abnormalities in temporal lobe epilepsy with and without mesial sclerosis. NeuroImage 46 (2), 353–9. http://dx.doi.org/10.1016/j.neuroimage.2009.02.020, 19249372.

Ng, S.Y., Villemagne, V.L., Masters, C.L., Rowe, C.C., 2007. Evaluating atypical dementia syndromes using positron emission tomography with carbon 11 labeled Pittsburgh Compound B. Archives of Neurology 64 (8), 1140–4. http://dx.doi.org/10.1001/archneur.64.8.1140, 17698704.

O'Toole, A.J., Jiang, F., Abdi, H., Pénard, N., Dunlop, J.P., Parent, M.A., 2007. Theoretical, statistical, and practical perspectives on pattern-based classification approaches to the analysis of functional neuroimaging data. Journal of Cognitive Neuroscience 19 (11), 1735–52. http://dx.doi.org/10.1162/jocn.2007.19.11.1735, 17958478.

Price, J.C., Klunk, W.E., Lopresti, B.J., Lu, X., Hoge, J.A., Ziolko, S.K., et al. 2005. Kinetic modeling of amyloid binding in humans using PET imaging and Pittsburgh Compound-B. Journal of Cerebral Blood Flow & Metabolism 25 (11), 1528–47. http://dx.doi.org/10.1038/sj.jcbfm.9600146, 15944649.

Rabinovici, G.D., Furst, A.J., Alkalay, A., Racine, C.A., O'Neil, J.P., Janabi, M., et al. 2010. Increased metabolic vulnerability in early-onset Alzheimer's disease is not related to amyloid burden. Brain 133 (2), 512–28. http://dx.doi.org/10.1093/brain/awp326.

Rabinovici, G.D., Furst, A.J., O'Neil, J.P., Racine, C.A., Mormino, E.C., Baker, S.L., et al. 2007. ^{11}C-PIB PET imaging in Alzheimer disease and frontotemporal lobar degeneration. Neurology 68 (15), 1205–12. http://dx.doi.org/10.1212/01.wnl.0000259035.98480.ed, 17420404.

Rabinovici, G.D., Jagust, W.J., Furst, A.J., Ogar, J.M., Racine, C.A., Mormino, E.C., et al. 2008. Abeta amyloid and glucose metabolism in three variants of primary progressive aphasia. Annals of Neurology 64 (4), 388–401. http://dx.doi.org/10.1002/ana.21451, 18991338.

Rabinovici, G.D., Rosen, H.J., Alkalay, A., Kornak, J., Furst, A.J., Agarwal, N., et al. 2011. Amyloid vs FDG-PET in the differential diagnosis of AD and FTLD. Neurology 77 (23), 2034–42. http://dx.doi.org/10.1212/WNL.0b013e31823b9c5e, 22131541.

Rachakonda, S., Liu, J., Calhoun, V. (2008), Fusion ICA Toolbox (FIT)

Rosen, H.J., Gorno-Tempini, M.L., Goldman, W.P., Perry, R.J., Schuff, N., Weiner, M., et al. 2002. Patterns of brain atrophy in frontotemporal dementia and semantic dementia. Neurology 58 (2), 198–208. http://dx.doi.org/10.1212/WNL.58.2.198, 11805245.

Rosenbloom, M.H., Alkalay, A., Agarwal, N., Baker, S.L., O'Neil, J.P., Janabi, M., et al. 2011. Distinct clinical and metabolic deficits in PCA and AD are not related to amyloid distribution. Neurology 76 (21), 1789–96. http://dx.doi.org/10.1212/WNL.0b013e31821cccad, 21525424.

Scheltens, P., Erkinjunti, T., Leys, D., Wahlund, L.O., Inzitari, D., del Ser, T., et al. 1998. White matter changes on CT and MRI: an overview of visual rating scales. European Task Force on Age-Related White Matter Changes. European Neurology 39 (2), 80–9. http://dx.doi.org/10.1159/000007921, 9520068.

Seeley, W.W., Crawford, R.K., Zhou, J., Miller, B.L., Greicius, M.D., 2009. Neurodegenerative diseases target large-scale human brain networks. Neuron 62 (1), 42–52. http://dx.doi.org/10.1016/j.neuron.2009.03.024, 19376066.

Sepulcre, J., Sabuncu, M.R., Becker, A., Sperling, R., Johnson, K.A., 2013. In vivo characterization of the early states of the amyloid-beta network. Brain: a Journal of Neurology 136 (7), 2239–52. http://dx.doi.org/10.1093/brain/awt146, 23801740.

Shirer, W.R., Ryali, S., Rykhlevskaia, E., Menon, V., Greicius, M.D., 2012. Decoding subject-driven cognitive states with whole-brain connectivity patterns. Cerebral Cortex (New York, N.Y.: 1991) 22 (1), 158–65. http://dx.doi.org/10.1093/cercor/bhr099, 21616982.

Smith, S.M., Fox, P.T., Miller, K.L., Glahn, D.C., Fox, P.M., Mackay, C.E., et al. 2009. Correspondence of the brain's functional architecture during activation and rest. Proceedings of the National Academy of Sciences of the United States of America 106, 13040–5. http://dx.doi.org/10.1073/pnas.0905267106, 19620724.

Tang-Wai, D.F., Graff-Radford, N.R., Boeve, B.F., Dickson, D.W., Parisi, J.E., Crook, R., et al. 2004. Clinical, genetic, and neuropathologic characteristics of posterior cortical atrophy. Neurology 63 (7), 1168–74. http://dx.doi.org/10.1212/01.WNL.0000140289.18472.15, 15477533.

Thomas, B.A., Erlandsson, K., Modat, M., Thurfjell, L., Vandenberghe, R., Ourselin, S., et al. 2011. The importance of appropriate partial volume correction for PET quantification in Alzheimer's disease. European Journal of Nuclear Medicine and Molecular imaging 38 (6), 1104–19. http://dx.doi.org/10.1007/s00259-011-1745-9, 21336694.

Tosun, D., Schuff, N., Mathis, C.A., Jagust, W., Weiner, M.W., 2011. Spatial patterns of brain amyloid-beta burden and atrophy rate associations in mild cognitive impairment. Brain: a Journal of Neurology 134 (4), 1077–88. http://dx.doi.org/10.1093/brain/awr044, 21429865.

Whitwell, J.L., Jack, C.R. Jr., Kantarci, K., Weigand, S.D., Boeve, B.F., Knopman, D.S., et al. 2007. Imaging correlates of posterior cortical atrophy. Neurobiology of Aging 28 (7), 1051–61. http://dx.doi.org/10.1016/j.neurobiolaging.2006.05.026, 16797786.

Zhang, S., Li, C.S., 2012. Functional connectivity mapping of the human precuneus by resting state fMRI. Neuroimage 59 (4), 3548–62. http://dx.doi.org/10.1016/j.neuroimage.2011.11.023, 22116037.

Zhou, J., Gennatas, E.D., Kramer, J.H., Miller, B.L., Seeley, W.W., 2012. Predicting regional neurodegeneration from the healthy brain functional connectome. Neuron 73 (6), 1216–27. http://dx.doi.org/10.1016/j.neuron.2012.03.004, 22445348.